

HIGH-FIDELITY SWEEP AND LEANED ROTOR BLADE DESIGN OPTIMIZATION USING EVOLUTIONARY ALGORITHM

Akira Oyama*

NASA Glenn Research Center, Brook Park, OH 44135, USA
(440) 962-3148, aoyama@dino.grc.nasa.gov

Meng-Sing Liou†

NASA Glenn Research Center, MS 5-11, Brook Park, OH 44135, USA
(216) 433-5855, meng-sing.liou@grc.nasa.gov

and

Shigeru Obayashi#

Tohoku University, Katahira 2-1-1, Sendai, Japan
+81-22-217-5265, obayashi@ieee.org

ABSTRACT

In this paper, aerodynamic blade design optimization for a transonic axial compressor has demonstrated by using an evolutionary-algorithm-based high-fidelity design optimization tool. The present method uses a three-dimensional Navier-Stokes solver named TRAF3D for aerodynamic analysis to represent flow fields accurately and the real-coded ARGGA for efficient and robust design optimization. The present method successfully obtained a design that reduced entropy production by more than 16% compared with the rotor67 while satisfying constraints on the mass flow rate and the pressure ratio. This study gave some insights into design optimization of a swept and leaned rotor blade for transonic axial compressors.

INTRODUCTION

Compressor is a critical part in developing a new aeroengine because a small improvement in efficiency can result in huge savings in yearly fuel costs of an aircraft fleet. Although today's aeroengine compressors have achieved very high performance, there is still an increasing demand for new compressor designs to achieve an even higher performance.

One approach to improve further compressor performance is to develop a computer-based design system using a high-fidelity flow solver and a numerical design optimization method. Currently, the state-of-the-art blade design systems depend on the axisymmetric through-flow method in the initial stage of the blade shape design. High-fidelity Computational Fluid Dynamics (CFD) such as the three-dimensional Navier-Stokes (N-S) solver may be also used, but often just for validation purposes or for evaluating losses coefficient to be used for the next through-flow calculation. Then, a blade design is manually optimized by trial and error basis by design experts by relying on their experiences and intuition. Such conventional approach, however, has nearly reached its limits. The

first reason is that the through-flow method cannot capture complicated flow structure inside a compressor such as secondary flow, shock/boundary layer interaction. Another reason is that a blade design for a compressor is very difficult to be solved by trial and error basis since it involves a large number of design parameters, multimodal and nonlinear objectives and constraints such as efficiency, total pressure ratio, and mass flow rate. Therefore, there is a demand for a revolutionary approach using three-dimensional N-S computations and an efficient and robust numerical design optimization method.

In [1], the authors successfully developed a high-fidelity numerical optimization tool for aerodynamic transonic axial-flow blade designs. In this tool, an evolutionary algorithm named real-coded adaptive-range genetic algorithm was adopted for efficient and robust design optimization. A three-dimensional N-S solver is used for aerodynamic analysis. To overcome expected difficulty in computational time, the computation was parallelized and performed on SGI ORIGIN 2000 clusters. Aerodynamic redesign of the NASA rotor 67 has demonstrated superiority of the method over the conventional design approach.

* NRC Research Associate, Turbomachinery and Propulsion System Division, Member AIAA. Located at Ohio Aerospace Institute ICOMP, 22800 Cedar Point Rd., Cleveland, OH 44142, USA

† Senior Scientist, Turbomachinery and Propulsion System Division, Associate Fellow AIAA

Professor, Institute of Fluid Science, Associate Fellow AIAA

Another approach to improve compressor performance is use of swept and leaned blades. It is known that axial sweep applied to a subsonic blade can improve efficiency by counteracting the development of the secondary flow through the blade channel², and axial sweep applied to a transonic or supersonic blade helps to reduce flow losses due to shock and shock/boundary layer interaction³. Circumferential lean is also known to influence strongly the development of the secondary flow in a compressor⁴. However, optimal swept and lean distributions for a transonic axial compressor blade are not well known.

Objective of the present paper is to give some insights into design optimization of a swept and leaned rotor blade for axial compressors. To achieve this goal, spanwise sweep and lean distributions of the NASA rotor 67 is demonstrated by using the high-fidelity design optimization tool.

DESIGN OPTIMIZATION PROBLEM

The optimization problem considered here is to seek a redesign of NASA rotor67⁵, which is a low-aspect-ratio transonic axial-flow fan rotor and is the first-stage rotor of a two-stage fan. The fan was designed and tested to help provide the technology to develop efficient, lightweight engines for short-haul aircraft in 1970s. The rotor 67 was designed by using a streamline-analysis computational procedure, which provides an axisymmetric, compressible-flow solution to the continuity, energy, and radial equilibrium equations.

The rotor design pressure ratio is 1.63 at a mass flow of 33.25 kg/sec. The design rotational speed is 16043 rpm, which yields a tip speed of 429 m/sec and an inlet tip relative Mach number of 1.38. The rotor has 22 blades and aspect ratio of 1.56 (based on average span/root axial chord). The rotor solidity varies from 3.11 at the hub to 1.29 at the tip. The inlet and exit hub/tip radius ratios are 0.375 and 0.478, respectively. Reynolds number is 1.797M based on the blade axial chord at the hub.

Objective of the aerodynamic rotor shape design optimization problem is to minimize the flow loss manifested via entropy generation. Here, mass-averaged entropy production from inlet to exit at the design point of rotor67 is considered as the objective function to be minimized. Because an optimized rotor design should meet the required mass flow rate and pressure ratio, they are maintained by specifying constraints on them:

$$\left| \frac{\text{massflowrate}_{\text{design}} - \text{massflowrate}_{\text{rotor67}}}{\text{massflowrate}_{\text{rotor67}}} \right| \leq 0.005 \quad (1)$$

$$\left| \frac{\text{pressureratio}_{\text{design}} - \text{pressureratio}_{\text{rotor67}}}{\text{pressureratio}_{\text{rotor67}}} \right| \leq 0.01 \quad (2)$$

HIGH-FIDELITY DESIGN OPTIMIZATION METHOD

The high-fidelity design optimization method for axial compressor blade developed by the authors in [1] is used for the present design optimization. Brief description of the method is presented in this section.

BLADE SHAPE PARAMETERIZATION

Here a rotor blade shape is represented by four blade profiles, respectively at 0%, 31%, 62%, and 100% spanwise stations (all spanwise locations discussed here are measured from the hub), the spanwise twist angle distribution, and the stacking line. Each of these sectional profiles can be uniquely defined by using a mean camber line and a thickness distribution. Here, they are parameterized by the third-order B-Spline curves and positions of control points of the B-Spline curves are considered as the design parameters. As illustrated in Fig. 1, five control points are used for the mean camber line. For the thickness distribution, two control points are added at the leading edge and the trailing edge so that these points represent leading edge and trailing edge radii, respectively. Chordwise locations of the control points at leading edge and trailing edge are frozen to zero and one, respectively. These profiles are linearly interpolated from hub to tip.

Stagger angles are define at 0%, 33%, 67%, and 100% spanwise stations and linearly interpolated. Spanwise chord length distribution remains same as that of the rotor 67. Final Blade shape is defined by stacking the blade profiles around the center of gravity of each profile. Here, the stacking line is defined by four lines as shown in the Fig. 2. As a result, each blade shape is represented with 66 design parameters.

THREE-DIMENSIONAL NAVIER-STOKES SOLVER FOR CASCADE FLOW

The three-dimensional N-S code used in the present research is TRAF3D^{6,7}. Capability of the present code has been validated by comparing the computed results to some experiments such as the Goldman annular vane with and without end wall contouring, the low speed Langston linear cascade⁶ as well as the NASA rotor67⁷.

TRAF3D solves the three-dimensional full Reynolds-averaged N-S equations. It uses a central-differencing scheme including artificial dissipation terms introduced by Jameson, Schmidt, and Turkel⁸ to maintain stability and to prevent oscillations near shocks or stagnation points. In order to minimize the amount of artificial diffusion inside the shear layer, the eigenvalues scaling of Martinelli⁹ and Swanson and Turkel¹⁰ are incorporated. The two-layer eddy-viscosity model of Baldwin and Lomax is adopted for the

turbulence closure. The system of the differential equations is advanced in time using an explicit four-stage Runge-Kutta scheme. In order to accelerate convergence of calculations, local time-stepping, implicit residual smoothing¹¹, and the Full Approximation Storage multigrid technique¹² are adopted.

At the subsonic axial inlet, the flow angles, total pressure and total enthalpy are specified according to the theory of characteristics while the outgoing Riemann invariant is taken from the interior. At the subsonic axial outlet, the average value of the static pressure at the hub is prescribed and the density and components of velocity are extrapolated together with the circumferential distribution of pressure. The radial equilibrium equation is used to determine the spanwise distribution of the static pressure. On sidewalls, the momentum equation, the no-slip condition, and the temperature condition are used to compute pressure and density. For the calculations presented in this paper, all the walls have been assumed to be adiabatic. The periodicity from blade passage to blade passage is imposed by setting periodic phantom cell values. At the wake, where the grid is not periodic, the phantom cells overlap the real ones. Linear interpolations are then used to compute the value of the dependent variables in phantom cell.

The three-dimensional grids are obtained by stacking two-dimensional grids generated on the blade-to-blade surface. These two-dimensional grids are of C-type and are elliptically generated, with controlled grid spacing and orientation at the wall. The problem of grid skewness due to high stagger or large camber is addressed by allowing the grid to be non-periodic on the wake¹³. By adding lines near the wall, viscous grids are obtained from the inviscid grids. The wall normal spacing scaled with the axial chord is 10^{-4} . In the spanwise direction a standard H-type structure has been adopted. Near the hub and tip walls geometric stretching is used for a specified number of grid points, after which the spanwise spacing remains constant. The number of the grid points is 201 chordwise x 53 tangential x 57 spanwise. Among the 201 chordwise grid points, 149 grid points are distributed along the blade shape. The computational grid for the NASA rotor 67 is shown in Fig. 3.

EVOLUTIONARY ALGORITHMS

Evolutionary Algorithms (EAs, see [14,15] for example) are relatively new optimization approach mimicking mechanism of the natural evolution, where a biological population evolves over generations to adapt to an environment by selection, recombination and mutation. In EAs, a design candidate, objective function values, and design variables usually correspond to an individual, fitness, and genes, respectively.

Starting with an initial population of design candidates, which is often generated by random sampling from the design space, EAs select good design candidates in terms of fitness. Typically, fitness of a design candidate is evaluated in terms of its objective function values. Then, recombination operator is applied the selected design candidates, where new design candidates are produced by exchanging features of the selected designs with the intent of improving the fitness of the next generation. Then, mutation is applied to design parameters of the new population to maintain diversity in the population.

One of the key features of EAs is that it searches from multiple points in the design space in contrast to the gradient-based methods that move from a single design point. In addition, EAs use objective function values alone to determine a search direction and do not require gradients of the objective function while the gradient-based methods use local gradient information of an objective function. These features lead to advantages such as the following:

- 1) Robustness: First of all, EAs handle any design problems that may involve non-differentiable objective function and/or a mix of continuous, discrete, and integer design parameters. EAs also have a capability to find a global optimum of a multimodal objective function.
- 2) Suitability to parallel computing: Because EAs are population-based search algorithms, all design candidates in each generation can be evaluated in parallel by using the simple master-slave concept. Parallel efficiency is expected to be extremely high, if objective function evaluations consume most of the computational time. High-fidelity compressor aerodynamic design optimization is a typical case.
- 3) Simplicity in coupling evaluation codes: Because EAs use only objective function values of design candidates, EAs do not need substantial modification or sophisticated interface to evaluation codes.
- 4) Straightforward application to multiobjective optimization problems: EAs find compromised optimum designs so-called Pareto-optimal solutions in parallel when applied to a multiobjective optimization problem.

In the present method, the real-coded Adaptive-Range Genetic Algorithm (real-coded ARGAs)^{16,17} is adopted. The real-coded ARGAs is an EA that can solve large-scale design optimization problems very efficiently by promoting the population toward promising design regions during the optimization process. The real-coded ARGAs has been successfully applied to airfoil design optimization¹⁶ and wing design optimization¹⁷. Feasibility of the real-coded ARGAs for high-fidelity compressor blade design optimization has

been also demonstrated in [1].

For the present optimization, unbiased initial population is generated by randomly spreading solutions over the entire initial design space. Fitness of each design candidate is determined by its rank among population of design candidates according to the objective function value and the extent of constraint violation using the constrained domination approach¹⁸ where each design candidate is ranked according to the following rule:

A solution i is better than a solution j , if any of the following condition is true:

1. Both solutions i and j satisfy the given constraints and solution i has smaller entropy production
2. Solution i satisfy the given constraints while solution j does not.
3. Both solutions i and j don't satisfy the given constraints, but solution i has a smaller constraint violation where constraint violation is defined as:

$$CV = 2 \cdot CV_{massflowrate} + CV_{pressureratio} \quad (8)$$

4. CFD computation of solution i converges while that of solution j does not.

Then, fitness of every design candidate is determined according to its rank as suggested by Michalewicz¹⁹. The constrained domination approach handles design constraints without using penalty function. In addition, this approach maintains sufficient selection pressure throughout the optimization.

The stochastic universal sampling method²⁰ is used for selection of potential parents of next generation design candidates where selection probability of each individual is assigned on the bias of its fitness and two potential parents are selected at once to avoid a stochastic aspect so-called genetic drift. Based on our experiences, the blended crossover (BLX-a) is selected for recombination of two potential parents to generate the next generation design candidates. The blended crossover is the most common approach for recombination of two parents represented by a vector of real numbers proposed by Eshelman and Schaffer²¹. Here, BLX-0.5 is used because both exploration and exploitation of the design space are carried out equally.

Mutation takes place at a probability of 10% and then adds a random disturbance to the corresponding gene. The present EA adopts the elitist strategy²² where the best and the second best individuals in each generation are transferred into the next generation without any recombination or mutation. The elitist strategy guarantees a monotonic improvement in the objective function value. From our experience, population size and number of generation are set to 64 and 100, respectively.

PARALLELIZATION

The main concern related to the use of an EA and a

three-dimensional N-S solver for an aerodynamic compressor design optimization problem is the required computational effort. Fortunately, powerful parallel computers are increasingly made available in many institutions and universities. In addition, EAs are intrinsically amenable to parallel algorithms and the computation can be easily parallelized. Furthermore, the PC clusters are emerging as a powerful and affordable alternative. Hence, the issue of computational cost is rapidly diminishing and yet, the ability of applying the EAs to complex problems is increasing. In the present study, all computations are performed on the SGI Origin2000 clusters consisting of 640 PEs located at the Institute of Fluid Science, Tohoku University in Japan. The total scalar performance and the total memory size are 384GLOPS and 640GB, respectively.

Here aerodynamic evaluation of design candidates at each generation is parallelized using the simple master-slave concept; the grid generations and the flow calculations associated to the design candidates of a generation are distributed into 64 PEs of the SGI Origin2000 clusters. The corresponding turnaround time is expected to be almost 1/64 of that needed on a single processor alone, because 1) grid generation and N-S computation of each design candidate of each generation can be computed independently, 2) computational time for CFD computation of each design candidate is almost identical, 3) Each N-S computation takes about nine hours of computational time on a SGI ORIGIN2000 PE while the real-coded ARGAs uses just a few seconds per each generation.

RESULTS

The first step of an EA-based design optimization is to properly define the design space. Even though the real-coded ARGAs does not require definition of the design space, it still needs initial design candidate distribution. In this study, the NASA rotor 67 is used as a baseline around which the initial candidates are populated. Specifically, the central values of the initial design space are made to correspond to the design parameter values representing the rotor 67 geometry. These values are found by minimizing geometry difference from rotor 67 by using the EA without any flow computation.

Table 1 presents performance of the optimized design and the NASA rotor 67. The optimized design successfully cut its entropy generation by more than 16% compared with NASA rotor 67 after 100 generations while satisfying the constraints on the mass flow rate and the total pressure ratio. This is a significant improvement for a compressor blade design. Figure 4 presents optimization history in terms of objective function value (entropy production).

Figures 5 and 6 compare spanwise leading-edge

sweep and lean distributions of the optimized design and the NASA rotor 67. While the rotor 67 has constant backward sweep, the optimized design has less backward sweep near the hub and larger backward sweep near the tip. This is probably because the flow loss due to shock wave is more significant near the tip than the hub. The optimized design also has larger lean toward pressure side near hub. Figure 7 compares stagger angle distributions. Although the distributions are qualitatively almost identical, the optimized design has larger stagger angle. The blade profiles of the optimized design and rotor67 are shown in Fig. 8.

Figure 9 compares spanwise entropy production distributions of rotor67 and the optimized design. The figure shows that the entropy production is reduced mainly in outboard of the mid-span.

Figures 10-13 compare blade profiles and surface static pressure distributions at 10%, 33%, 67%, and 90% spanwise stations, respectively. To reduce the excessive flow accelerations near the leading edge at 10% and 33% spans, the optimized design has decreased incidence angles. In addition, two weak shock waves are produced instead of single strong shock wave at 67% span to reduce entropy production due to shock wave. The shock wave at 90% span is also significantly weakened.

Figures 14-17 present the corresponding relative Mach number contours. At 10% and 33% spans, supersonic bubble on the suction side near the leading edge of the optimized design has almost disappeared. This explains the reduction in entropy production between the hub and the midspan. The two shock waves at 67% span shown in Fig.12 are recognized in Fig. 16. At 90% station, the bow shock impinging the blade suction side and its reflection shock have become significantly weakened to reduce entropy production through the shocks.

Figure 18 compares oil flow patterns and static pressure contours on suction surfaces of rotor 67, the current design, and the optimized design presented in [1] where only profile shapes were optimized (with fixed stagger angle distribution and stacking line).The current optimized design is characterized by the lambda-shaped shock on the suction side, which reduces entropy production due to the shock wave by having two weaker shock waves in the mid-span. On the other hand, previous design has single shock wave that is more tilted and weaker than that of the rotor 67 to reduce the shock-generated entropy. The current design is better than the previous optimized design in the sense that the oil flow appears to be more 2D and to have smaller separated region.

Figure 19 shows the performance maps of the optimized designs and rotor 67. Although optimization is carried out for the designed operating condition (33.774kg/sec), it is remarkable that the current design

still maintains higher isentropic efficiency over most of the range of operating conditions achieving a remarkable, almost 2% improvement in adiabatic efficiency. On the other hand, the current design has slightly less peak adiabatic efficiency than the previous design. One of the reasons is probably premature convergence due to increased complexity of the current optimization problem. Larger population size and/or more generations of optimization may be necessary to obtain a better design. Another reason may come from the less smooth lean and sweep distributions of the current design than those of the rotor67 and the previous optimized design. Some smoothing before generating grids may be necessary. This figure also shows that maximum mass flow rate of the current design is smaller than that of the rotor 67 and the previous design because of the increased axial sweep while it satisfies the given constraint on the mass flow rate.

Total computation time of the current design optimization was 1515 hours (two month). Although parallel efficiency was expected to be almost 100%, the actual parallel efficiency was 73% on average (varied from 58% to 85%). The discrepancy between expected and actual parallel efficiencies comes from structure of the Origin2000 clusters. Each node of the clusters has two Processing Elements (PEs) and one shared memory. When a CFD computation is submitted to a node with both PEs free, the process is done very fast because the process occupies its memory. On the other hand, when a CFD computation is submitted to a node with one PE free and one PE occupied by other process, the computation becomes slower because it competes with the existing process for access to the memory. As a result, significantly different computational time of each CFD computation degraded parallel efficiency of the present computation. The present parallel efficiency, however, is still very high for parallel computation using 64 PEs. The parallel efficiency would be higher than 85% if a parallel computer with one memory per one PE was used. This result proves that EA-based high-fidelity compressor blade design optimization is extremely suitable for parallel computation.

CONCLUSIONS

In this paper, design optimization of spanwise sweep and lean distributions of the NASA rotor 67 is demonstrated by using the EA-based high-fidelity design optimization tool developed by the authors. In the present method, a three-dimensional N-S solver was used for aerodynamic analysis to represent flow fields accurately and produce reliable designs. The present method also adopts the real-coded ARGGA for efficient and robust design optimization.

The present study gave some insights into design optimization of a swept and leaned rotor blade for axial compressors. The optimized design has more backward sweep near the tip and less backward sweep near the hub. Flow structure around the current design is characterized by the lambda-shaped shock on the suction side, which reduces entropy production due to the shock wave by having two weaker shock waves in the mid-span region. Also the present study showed that swept blades tend to have smaller operating and maximum mass flow rate. Strict constraint on the mass flow rate is necessary for a sweep and lean distribution optimization.

Total computation time of the current design optimization was about two month. One may think the present approach is not affordable due to the expense. However, Moore's Law is supposed to continue for at least another 10 years according to Dr. Gordon E. Moore's speech at the 2003 International Solid-States Circuits Conference. This kind of computation will be easily demonstrated on a personal computer in the next 10 years.

ACKNOWLEDGEMENTS

The authors thank Drs. L. M. Larosiliere and R. V. Chima at NASA Glenn Research Center for their valuable advices in defining the present design optimization problem, and Dr. E. R. McFarland for managing the project. The authors also thank Dr. M. Marconcini at University of Florence for his help in using the TRAF3D code. The generosity of Institute of Fluid Science, Tohoku University for providing computational time on the SGI ORIGIN2000 cluster is greatly appreciated. This work was performed while the first author held a National Research Council Research Associateship Award at NASA Glenn Research Center.

REFERENCES

- 1) Oyama, A, Liou, M.-S., and Obayashi, S., "Transonic Axial-Flow Blade Shape Optimization Using Evolutionary Algorithm and Three-Dimensional Navier-Stokes Solver," AIAA Paper 2002-5642, 2002.
- 2) Yamaguchi, N., Tominaga, T., Hattori, S. and Mitsubishi, T., "Secondary-Loss Reduction by Forward-Skewing of Axial Compressor Rotor Blading," Proceedings of 1991 Yokohama International Gas Turbine Congress, Vol. 2, pp. 61-68.
- 3) Hah, C., Puterbaugh, S. L., and Wadia, A. R., "Control of Shock Structure and Secondary Flow Field Inside Transonic Compressor Rotors Through Aerodynamic Sweep," ASME Paper 98-GT-561, 1998.
- 4) Smith, L. H. Jr., "The Radial-Equilibrium Equation of Turbomachinery," *ASME Journal of Engineering for Power*, Vol. 88, No. 1, January 1966, pp.1.
- 5) Walter, S. C., William, S., and Donald, C. U., "Design and Performance of a 427-Meter-Per.-Second-Tip-Speed Two-Stage Fan Having a 2.40 Pressure Ratio," NASA TP-1314, October 1978.
- 6) Arnone, A., Liou, M.-S., and Povinelli, L. A., "Multigrid Calculation of Three-Dimensional Viscous Cascade Flows," NASA TM-105257, ICOMP-91-18, 1991.
- 7) Arnone, A., "Viscous Analysis of Three-Dimensional Rotor Flow Using a Multigrid Method," *ASME Journal of Turbomachinery*, Vol. 116, July 1994, pp. 435-445.
- 8) Jameson, A., Schmidt, W., and Turkel, E., "Numerical Solutions of the Euler Equations by Finite Volume Methods Using Runge-Kutta Time-Stepping Schemes," AIAA Paper 1981-1259, 1981.
- 9) Martinelli, L. and Jameson, A., "Validation of a Multigrid Method for the Reynolds Averaged Equations," AIAA Paper 1988-0414, 1988.
- 10) Swanson, R. C., and Turkel, E., "Artificial Dissipation and Central Difference Schemes for the Euler and Navier-Stokes Equations," AIAA Paper 1987-1107, 1987.
- 11) Jameson, A., "The Evolution of Computational Methods in Aerodynamics," *Journal of Appl. Mech.*, Vol. 50, 1983.
- 12) Jameson, A., "Transonic Flow Calculations," MAE Report 1651, MAE Department, Princeton University, July 1983.
- 13) Arnone, A., Liou, M.-S., and Povinelli, L. A., "Transonic Cascade Flow Calculations Using Non-Periodic C-Type Grids," Computational Fluid Dynamics Symposium on Aeropropulsion, NASA Lewis Research Center, Cleveland, April, 1990.
- 14) Miettinen, K., Makela, M. M., Neittaanmaki, P. and Periaux, J. (eds.), *Evolutionary Algorithms in Engineering and Computer Science*, John Wiley & Sons Ltd, Chichester, U.K., 1999.
- 15) Dasgupta, D. and Michalewicz, Z. (eds.), *Evolutionary Algorithms in Engineering Applications*, Springer-Verlag, Berlin, Heidelberg, 1997.
- 16) Oyama, A, Obayashi, S. and Nakahashi, K., "Real-Coded Adaptive Range Genetic Algorithm and Its Application to Aerodynamic Design," *JSME International Journal*, Series A, Vol. 43, No. 2, pp. 124-129, February 2000.
- 17) Oyama, A., Obayashi, S. and Nakamura, T., "Real-Coded Adaptive Range Genetic Algorithm Applied to Transonic Wing Optimization," *Applied Soft Computing*, Vol. 1, No. 3, pp. 179-187, 2001, <http://www.elsevier.com/locate/asoc> .

- 18) Deb, K., Pratap, A. and Moitra, S., "Mechanical Component Design for Multiple Objectives Using Elitist Non-Dominated Sorting GA," *Lecture Notes in Computer Science 1917 Parallel Problem Solving from Nature – PPSN VI*, edited by Schoenauer, M., Deb, K., Rudolph, G., Yao, X., Lutton, E., Merelo, J. J., and Schwefel, H.-P., Springer, Berlin, Germany, 2000, pp.859-868.
- 19) Michalewicz, Z., *Genetic Algorithms + Data Structures = Evolution Programs*, third revised edition, Springer-Verlag, Berlin, 1996.
- 20) Baker, J. E., "Reducing Bias and Inefficiency in the Selection Algorithm," *Proceedings of the Second International Conference on Genetic Algorithms*, Morgan Kaufmann Publishers, Inc., San Mateo, California, 1987, pp 14-21.
- 21) Eshelman, L. J. and Schaffer, J. D., "Real-Coded Genetic Algorithms and Interval Schemata," *Foundations of Genetic Algorithms.2*, Morgan Kaufmann Publishers, Inc., San Mateo, California, 1993, pp 187-202.
- 22) De Jong, K. A., "An Analysis of the Behavior of a Class of Genetic Adaptive Systems," Doctoral Dissertation, University of Michigan, Ann Arbor, 1975.

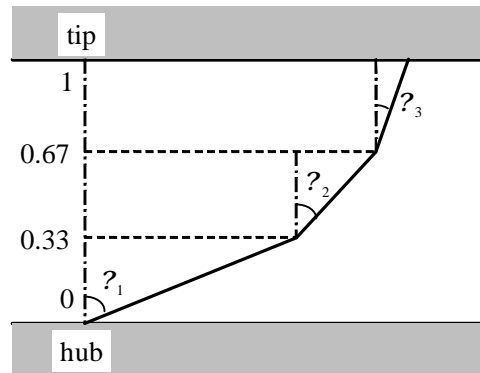


Figure 2. Stacking line definition.

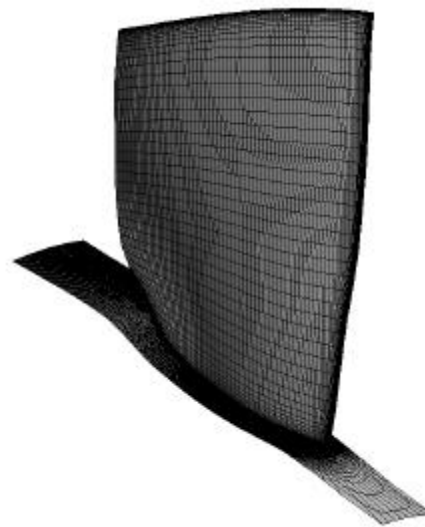


Figure 3. Computational grid over NASA rotor67.

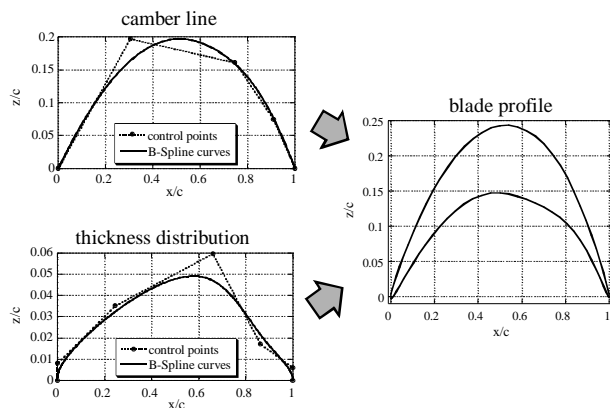


Figure 1. B-Spline curves for mean camber line and thickness distribution and the resultant blade profile.

Table 1. Computed performance of the optimized design and the NASA rotor 67.

	mass flow [kg/sec]	isentropic efficiency	pressure ratio	entropy production
NASA rotor67	33.774	0.91890	1.6758	0.0090467
Current optimum	33.621	0.93134	1.6672	0.0075459
Upper constraint	33.943		1.6926	
Lower constraint	33.605		1.6590	

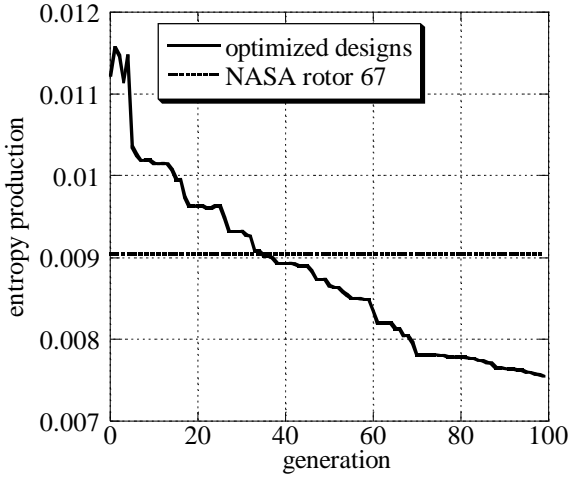


Figure 4. Optimization history.

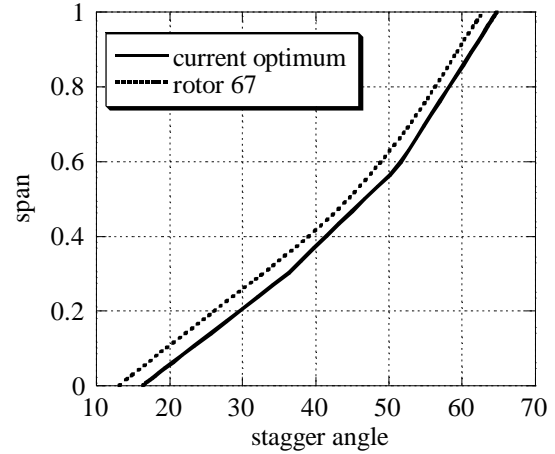


Figure 7. Comparison of the axial sweep distributions.

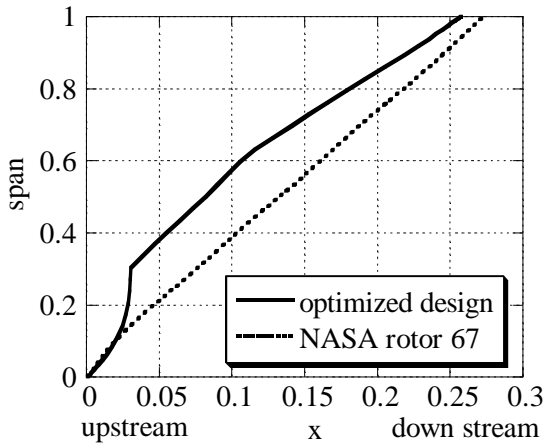


Figure 5. Comparison of the axial sweep distributions.

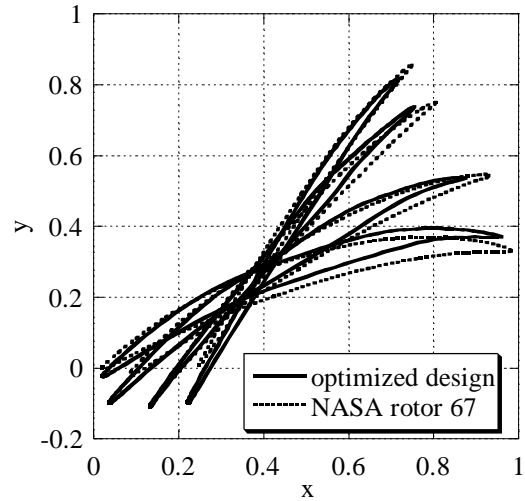


Figure 8. Blade profiles of the optimum design and rotor67.

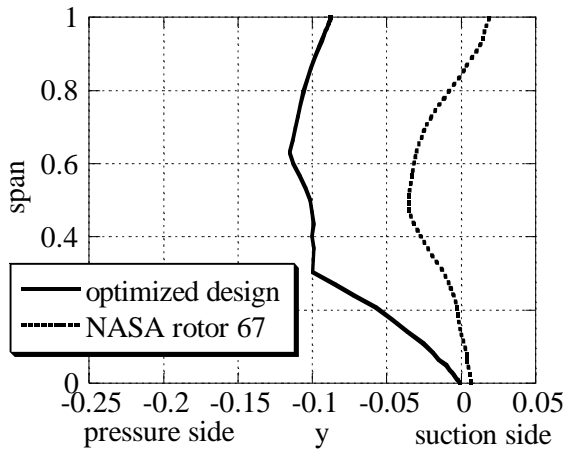


Figure 6. Comparison of the circumferential lean distributions.

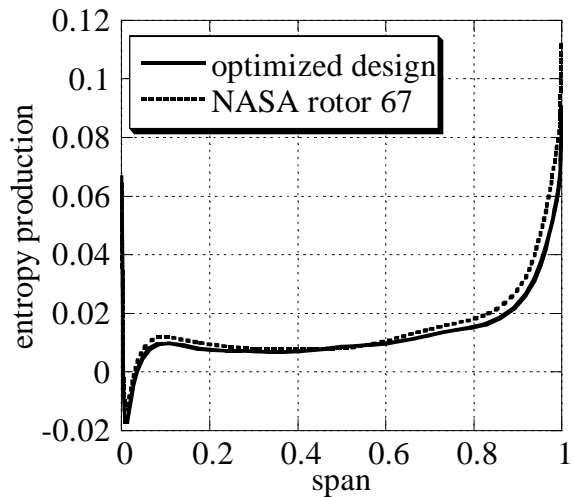


Figure 9. Comparison of spanwise entropy production distribution.

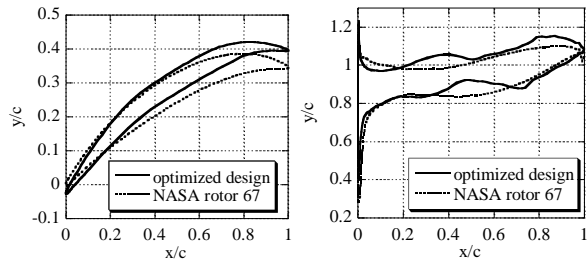


Figure 10. Comparison between the optimized design and the rotor 67 at 10% span.

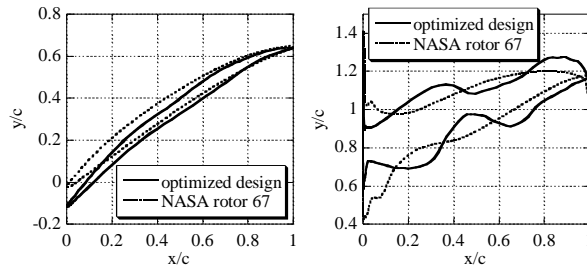


Figure 11. Comparison between the optimized design and the rotor 67 at 33% span.

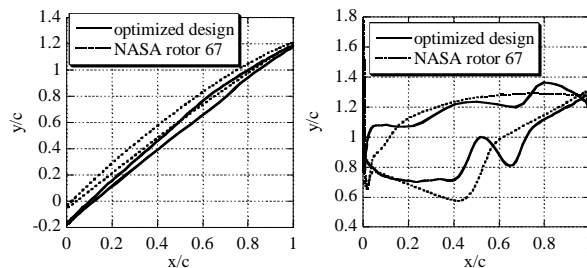


Figure 12. Comparison between the optimized design and the rotor 67 at 67% span.

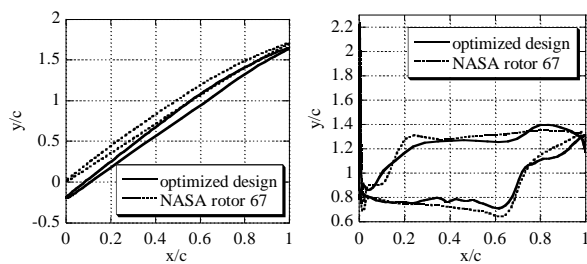


Figure 13. Comparison between the optimized design and the rotor 67 at 90% span.

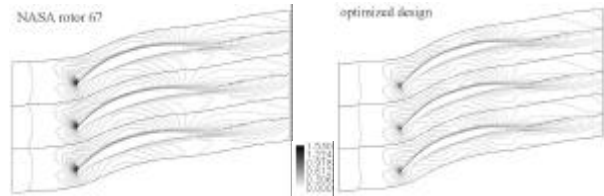


Figure 14. Relative Mach number contours at 10% span.

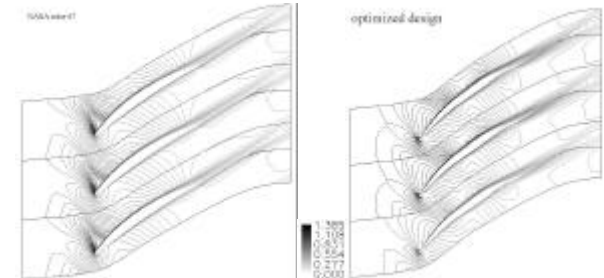


Figure 15. Relative Mach number contours at 33% span.

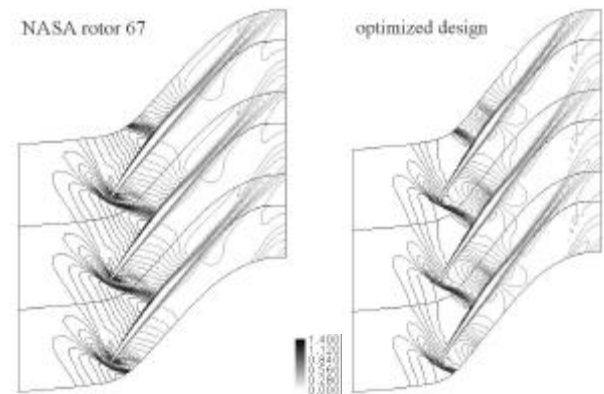


Figure 16. Relative Mach number contours at 67% span.

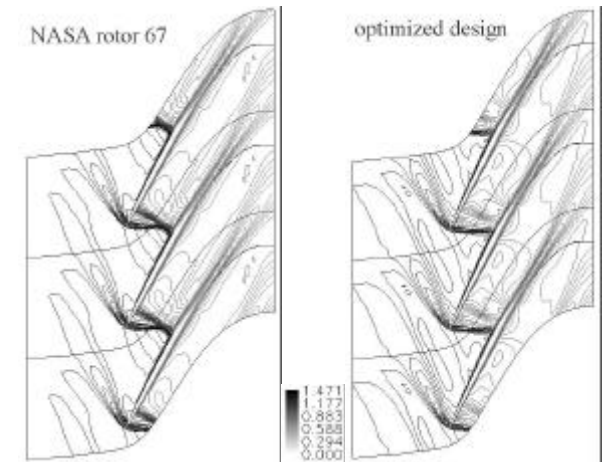


Figure 17. Relative Mach number contours at 90% span.

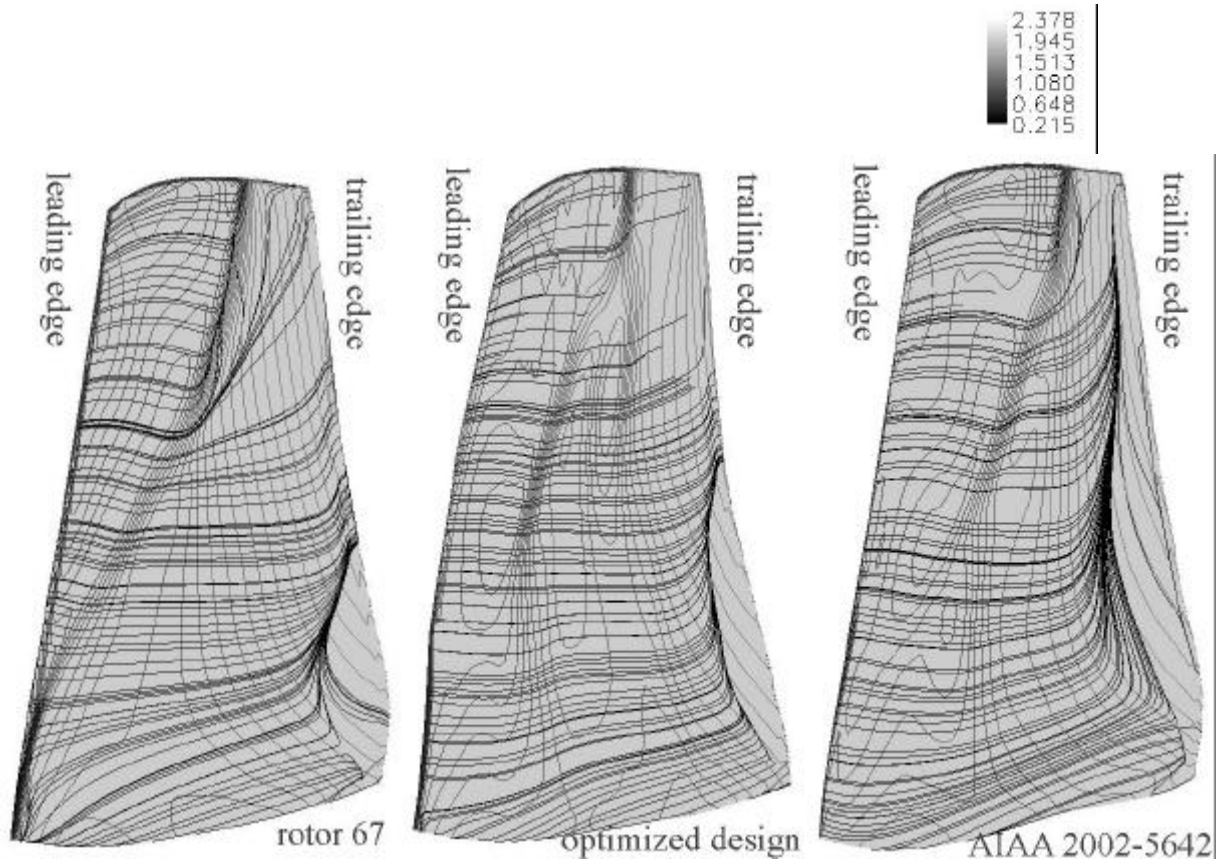


Figure 18. Oil flow patterns and static pressure contours on suction surfaces.

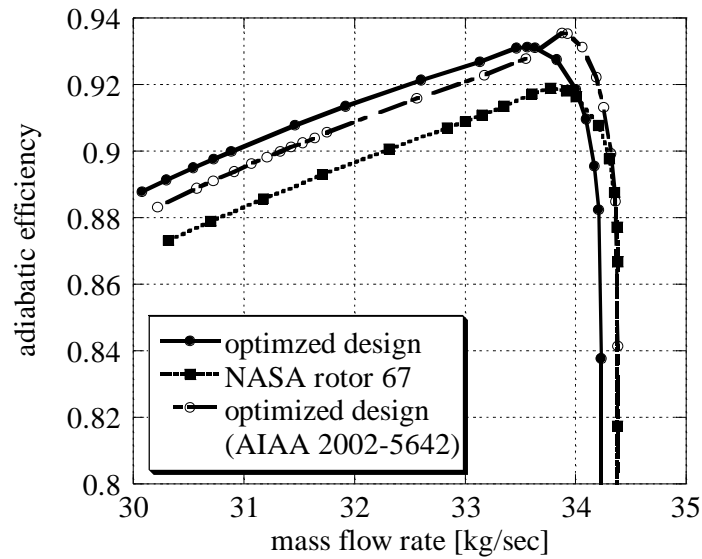


Figure 19. Performance map comparison between rotor67 and the optimum design.